Int. J. Bio-Inorg. Hybr. Nanomater., Vol. 4, No. 1 (2015), 49-54

ISSN Print: 2251-8533
ISSN Online: 2322-4142

International Journal of Bio-Inorganic Hybrid Nanomaterials

Low Temperature Hydrothermal Synthesis and Characterization and Optical Properties of $Sr_5Nb_4O_{15}$ – Nb_2O_5 Nanocomposite

Shahin Khademinia[1], Mahdi Behzad[2*], Abdolali Alemi[3], Mahboubeh Dolatyari[4]

[1] Ph.D., Department of Chemistry, Semnan University, Semnan 35351-19111, Iran

[2] Associate Professor, Department of Chemistry, Semnan University, Semnan 35351-19111, Iran

[3] Professor, Department of Inorganic Chemistry, Faculty of Chemistry, University of Tabriz, Tabriz, Iran

[4] Associate Professor, Laboratory of Nano Photonics & Nano Crystals, School of Engineering-Emerging Technologies, University of Tabriz, Tabriz, Iran

Received: 14 December 2014; Accepted: 17 February 2015

ABSTRACT

$Sr_5Nb_4O_{15}$ – Nb_2O_5 nanocomposites were synthesized in 2 and 4 M KOH aqueous solutions, via a non-stoichiometric 1:2 Sr:Nb molar ratio hydrothermal method at 160°C for 48 h (S_1 and S_2, respectively). $Sr(NO_3)_2$ and Nb_2O_5 were used as raw materials. The synthesized nanomaterials were characterized by powder X-Ray diffraction (PXRD) technique. It was found that $Sr_5Nb_4O_{15}$ has been crystallized in hexagonal crystal structure with space group P-3m1. Nb_2O_5 lattice parameters were also found as a= 6.175 Å, b= 29.175 Å, and c= 3.93 Å and a= 12.73 Å, b= 5.56 Å, and c= 4.88 Å with γ= 105.1°, respectively for the orthorhombic and monoclinic crystal structures. The morphologies of the synthesized materials were studied by field emission scanning electron microscope (FESEM). The FESEM images showed that the S_1 and S_2 nanocomposites had flower and plate like structures, respectively. Ultraviolet–Visible (UV-Vis) spectra analyses showed that the synthesized nanocomposites had strong light absorption properties in the ultraviolet light region. FTIR spectra of the obtained nanomaterials were also studied. Cell parameter refinements of the synthesized nanocomposites were also investigated.

Keyword: $Sr_5Nb_4O_{15}$; Hydrothermal Method; PXRD; Nanocomposite; Optical Property; Celref.

1. INTRODUCTION

Ceramics with general formula $A_5B_4O_{15}$ or $A_mB_{m-1}O_{3m}$ represent cubic perovskite structures. They are called cation-deficient perovskites and are subject of interest because of their properties such microwave dielectric [1], high relative permittivity, and low temperature coefficient of resonator frequency [4]. Among them, $Sr_5Nb_4O_{15}$ has been investigated for diamagnetic insulator [4-5]. Several methods have been reported for the synthesis of $Sr_5Nb_4O_{15}$ nanomaterials such as reaction sintering process [2], solid state reaction [3, 5 and 6], pyrolysis, and calcinations [7]. In the present study, a hydrothermal route was employed successfully for the

(*) Corresponding Author - e-mail: mbehzad@semnan.ac.ir

synthesis of nanostructured $Sr_5Nb_4O_{15}$ – Nb_2O_5 composites using $Sr(NO_3)_2$, Nb_2O_5 and KOH as raw materials. To the best of our knowledge, there is no report on the synthesis of nanostructured $Sr_5Nb_4O_{15}$ – Nb_2O_5 composites by this method. The effects of KOH concentration on the final products in phase composition and particle morphology were investigated, and the band gap energy of the as-prepared nanocomposites samples was initially estimated from UV-Visible spectra. Besides, FTIR spectra of the synthesized nanocomposites were also studied.

2. EXPERIMENTAL

2.1. Materials and methods

All chemicals including $Sr(NO_3)_2$, Nb_2O_5 and KOH were of analytical grade and were obtained from commercial sources (Merck, Germany) and were used without further purifications. The nanomaterials S_1 and S_2 were synthesized via hydrothermal method in 2 and 4M KOH aqueous solutions, respectively. Phase identifications were performed on a powder X-Ray diffractometer D5000 (Siemens AG, Munich, Germany) using CuK_α radiation. The morphology of the obtained materials was examined with a field emission scanning electron microscope (Hitachi FE-SEM model S-4160). Absorption spectra were recorded on a Jena Analytik Specord 40 (AnalytikJena UK, Wembley, UK). Also, FTIR spectra were recorded on a Tensor 27 (Bruker Corporation, Germany). Cell parameter refinement was reported by celref software version 3 (Laboratoire des Materiaux et du Génie Physique de l'Ecole Supérieure de Physique de Grenoble).

2.2. Hydrothermal synthesis of $Sr_5Nb_4O_{15}$- Nb_2O_5 nanocomposites

In typical synthetic experiments in both methods, 0.16 g (0.75 mmol) of $Sr(NO_3)_2$ (Mw = 211.62 g mol^{-1}) and 0.20 g (0.75 mmol) of Nb_2O_5 (Mw = 265.82 g mol^{-1}) were used. The raw materials were added to 50 mL of hot aqueous solutions of 2 or 4 M KOH (S_1 and S_2, respectively) under magnetic stirring at 80°C. The resultant solutions were stirred for further 15 min and transferred to a 100 mL Teflon lined stainless steel autoclave. The autoclave was sealed and heated at 160°C for 48 h. When the reaction was completed, it was cooled to room temperature by water immediately. The prepared powder was washed with distilled water and dried at 120°C for 20 min under normal atmospheric conditions and a cream like powder was collected for further analyses.

3. RESULTS AND DISCUSSION

3.1. Powder X-Ray diffraction analysis

The X-Ray diffraction patterns of the $Sr_5Nb_4O_{15}$–Nb_2O_5 nanocomposites samples are reported in Figures 1 and 2. Figure 1 shows the X-Ray diffraction (XRD) analysis of $Sr_5Nb_4O_{15}$ sample obtained in the θ-2θ geometry with Cu-K_α radiation. The results showed that the

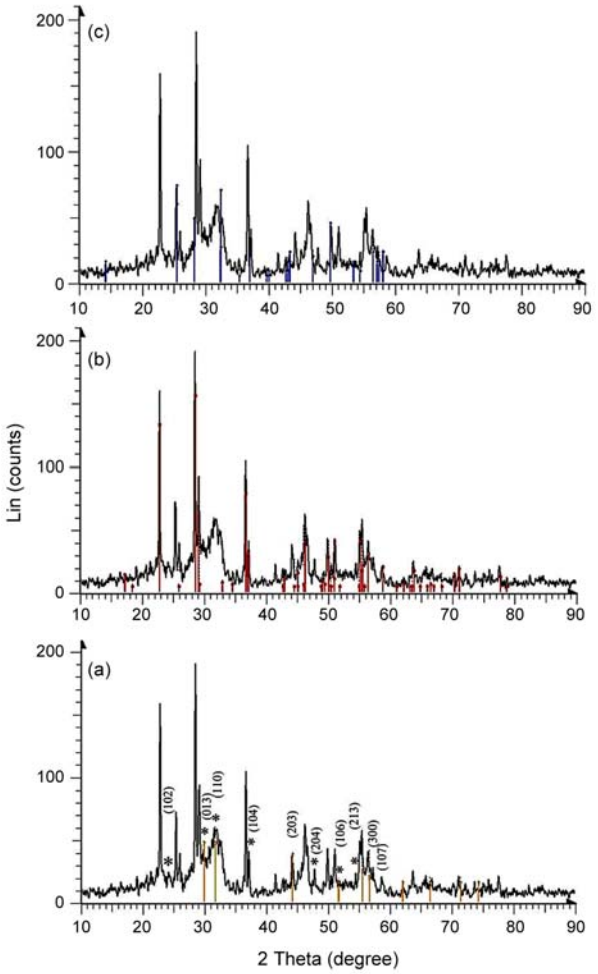

Figure 1: *PXRD patterns of the S_1. The bars show the Bragg's positions for a) $Sr_5Nb_4O_{15}$, b) orthorhombic Nb_2O_5 and c) monoclinic Nb_2O_5.*

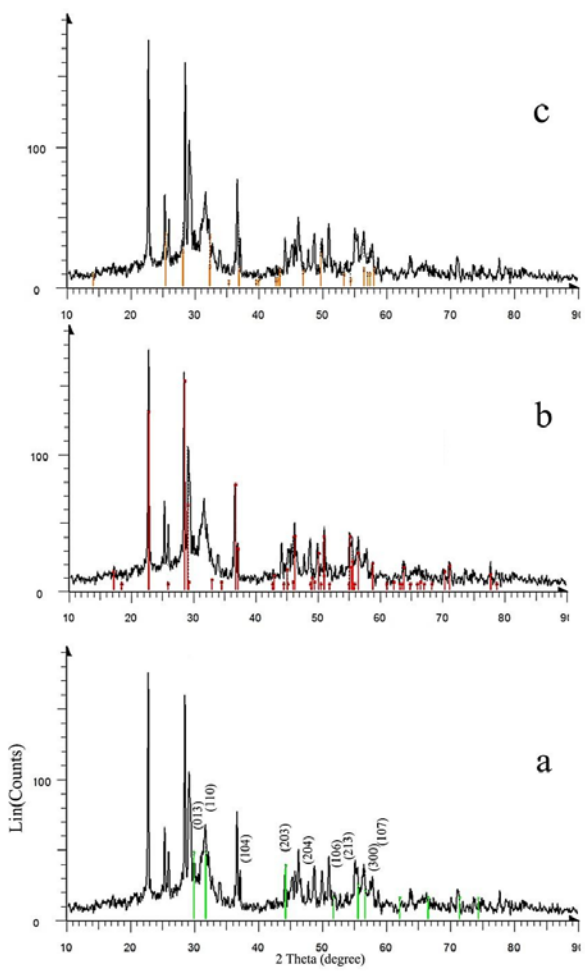

Figure 2: *PXRD patterns of the S_2. The bars show the Bragg's positions for a) $Sr_5Nb_4O_{15}$, b) orthorhombic Nb_2O_5 and c) monoclinic Nb_2O_5.*

pattern had two $Sr_5Nb_4O_{15}$ and Nb_2O_5 as main phases. $Sr_5Nb_4O_{15}$ structure was detected with hexagonal crystal structure which has been crystallized in the P3-m1 space group [1]. Two different crystal structures were observed for Nb_2O_5 in both (S_1) and (S_2) samples; namely orthorhombic and monoclinic crystal structures. Nb_2O_5 lattice parameters were found as a= 6.175 Å, b= 29.175 Å, and c= 3.93 Å and a= 12.73 Å, b= 5.56 Å, and c= 4.88 Å with γ= 105.1°, respectively for the orthorhombic and monoclinic crystal structures. It is also clear that according to the PXRD pattern, the $Sr_5Nb_4O_{15}$ phase formation compared to Nb_2O_5 phase is about 30%. Figure 2 shows that with changing the synthesis condition, there is still a mixture of two phases including $Sr_5Nb_4O_{15}$ and Nb_2O_5. The measured XRD data are in agreement with those of reported XRD for $Sr_5Nb_4O_{15}$ nanomaterials [1]. According to the PXRD patterns, it was found that the $Sr_5Nb_4O_{15}$ phase formation compared to Nb_2O_5 is about 45%. So it is clear that there is an optimization in $Sr_5Nb_4O_{15}$ phase formation with increasing KOH concentration. Compared to the nanomaterials of the hydrothermally synthesized $Sr_5Nb_4O_{15}$ (S_1), the diffraction lines in the powder XRD patterns of the $Sr_5Nb_4O_{15}$ – Nb_2O_5 nanocomposites (S_2) has shifted to lower 2θ values and therefore to the higher d values. So, using the peak with miller indices of 110, a blue diffraction line shift of Δ2θ = 31.52° (S2) – 31.78° (S_1) = -0.26° (Δd = 2.8308 Å (S2) – 2.8133 Å (S_1) = 0.0175Å) are calculated via Bragg's equation. So there is an expansion in the unit cell according to the calculated data.

Table 1 shows that refined cell parameter data for (S_1) and (S_2), respectively. The data showed that with changing the synthesis rout, the cell parameters for (S_2) were larger than those of (S_1). So there should be an expansion in the unit cell. It is in agreement with the interplanar spacing data calculated via Bragg's equation.

3.2. Morphology of the materials

Figure 3 shows typical FESEM images of the hydrothermally synthesized $Sr_5Nb_4O_{15}$ – Nb_2O_5 nanocomposites in 2M KOH solution (S_1). From the typical FESEM images of S_1 at low magnification in Figures 3a and b, it was found that the morphology of the obtained materials was in flake-like form. At higher

Table 1: *Cell parameter data for samples 1 and 2.*

Cell parameter	Standard Sample [3]	$Sr_5Nb_4O_{15}$ (S_1)	$Sr_5Nb_4O_{15}$ (S_2)
a	9.79601	9.8064	9.9136
b	5.65701	5.6526	5.7995
c	11.42101	11.3809	11.4237

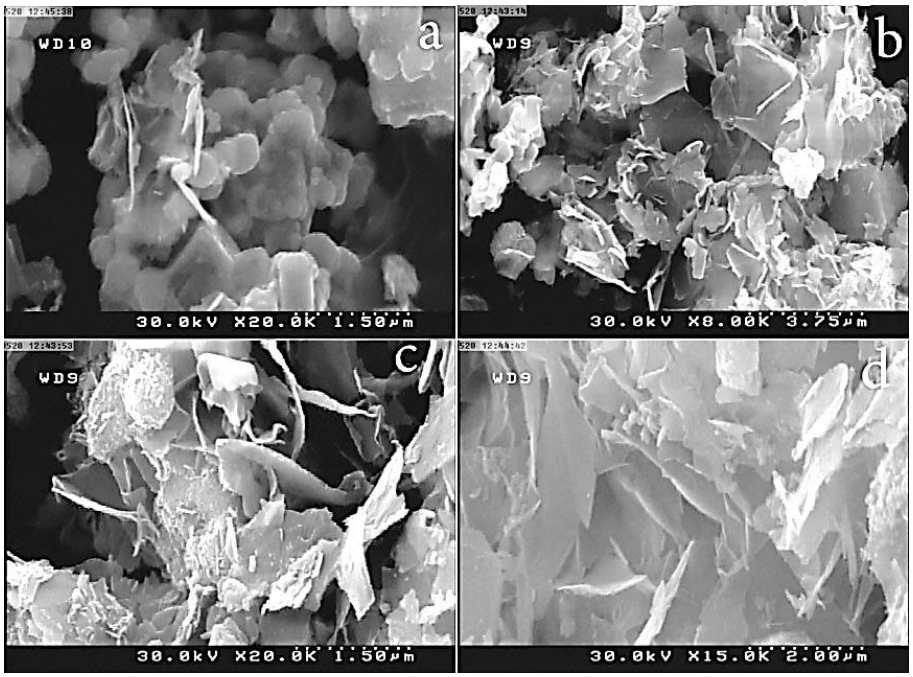

Figure 3: *FESEM images of S_1.*

magnification in Figures 3c and d, it is clear that the thickness sizes of the flakes are in the range of about 70 to 150 nm.

Figure 4 shows typical FESEM images of the hydrothermally synthesized $Sr_5Nb_4O_{15}$ – Nb_2O_5 nanocomposites in 4M KOH solution (S_2). FESEM images of S_2 in Figures 4a and b showed that the morphology of the obtained materials was in a mixture of flower structures from rods as petals. The small flower structures from the very small plates as petals crossed each

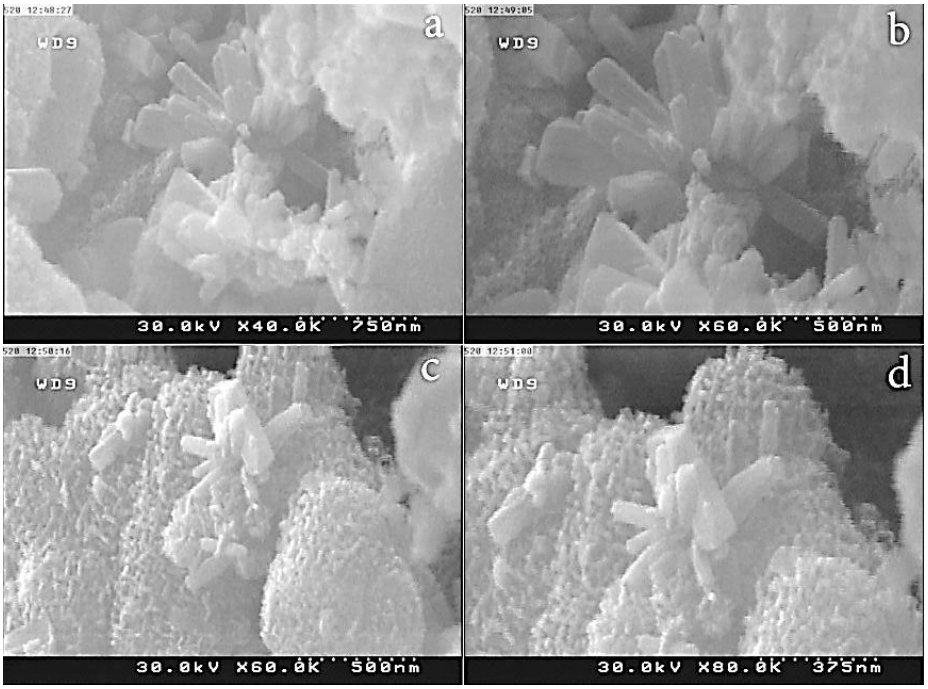

Figure 4: *FESEM images of S_2.*

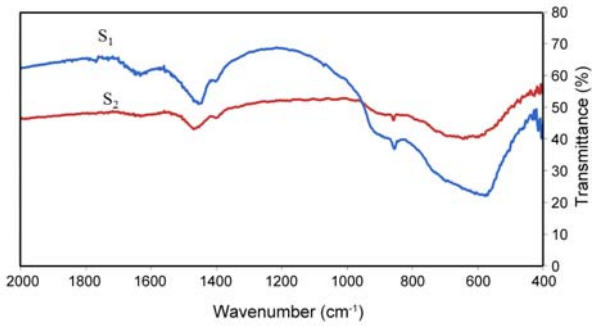

Figure 5: *FTIR spectra of S_1 and S_2.*

other formed the other like flower structures. Figures 4c and d show that the length sizes of the rod structures was in a range of about 150 to 300 nm. The thickness size of the rods was about 50 to 150 nm. So the images showed that the size ranges of the obtained materials were nearly non-homogeneous. Also, Figure 3d showed that the thickness size of the very small plates was in a range of about 37 to 50 nm.

Figure 5 shows the FTIR spectra of the synthesized S_1 and S_2 nanocomposites. The FTIR spectra obtained on the samples S_1 and S_2 show main absorptions bands at around 621, 644, 858, 1402, 1469 cm^{-1} and 566, 854, 1398, 1454, 1645 cm^{-1}, respectively, that are characteristic for the synthesized $Sr_5Nb_4O_{15}$ – Nb_2O_5 nanocomposites. The bands at around 650 and 850 cm^{-1} are assigned to monoclinic Nb_2O_5 and the bands at around 550 cm^{-1} is attributed to orthorhombic Nb_2O_5 [8-11]. It is a confirmation of the co-existence of both orthorhombic and monoclinic Nb_2O_5 in the synthesized nanocomposite that is in agreement with the measured PXRD data. The weak bands at around 1450 and 1640 cm^{-1} are attributed to the bending mode of H_2O molecules. The band at around 620 cm^{-1} is assigned to Sr – O vibration [12-14].

Figure 6 shows the UV-Vis spectra of the synthesized nanocomposites. The absorption peak positions in both spectra suggest that these materials are wide band gap semiconductors. It is clear in Figure 6a that there are three absorption bands at 208, 222, 253 and a shoulder at 270 nm. The absorption edge band is at about 360 nm and so the calculated band gap is about 3.44 eV. However, in Figure 6b there are the bands at 210, 285 and a weak band at 337 nm. The absorption edge band is at about 385 nm and so the calculated band gap is about 3.22 eV that is smaller than that of

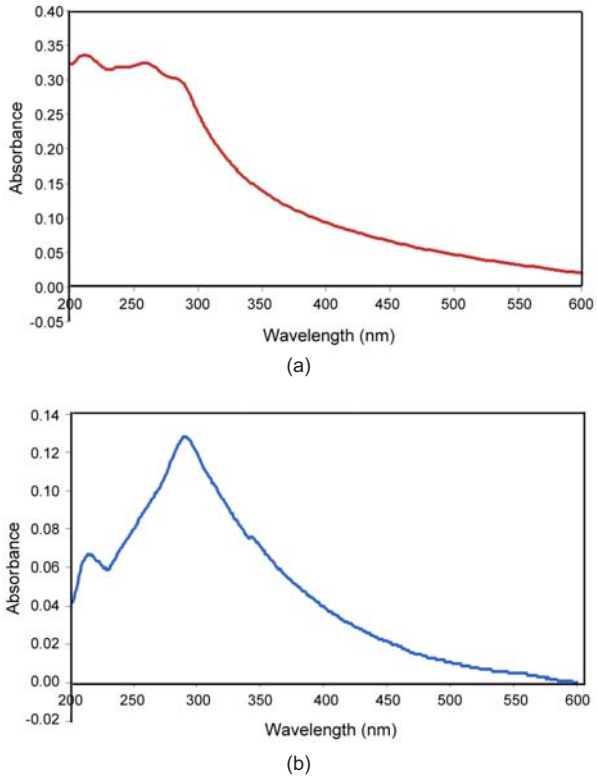

Figure 6: *UV-Vis spectra of S_1 (a) and S_2 (b).*

S_1. It is not surprising to observe the difference in the optical property because these two specimens have different constituting crystalline phases. However, it is clear that the absorption spectrum shown in Figure 5a is almost like that of Nb_2O_5 that is because of the very large Nb_2O_5/$Sr_5Nb_4O_{15}$ phase ratio [15]. Also, it is nearly like the other Sr-Nb-O mixed metal oxides absorption spectra. However, the band gaps are different from the calculated data in this work [16].

4. CONCLUSIONS

In this work, $Sr_5Nb_4O_{15}$ – Nb_2O_5 nanocomposites were synthesized successfully via hedrothermal method. PXRD patterns showed that the synthesis was successfull. FESEM images showed that the as-synthesized materials were in flake like (S_1) and two kind flower like structures (S_2). UV-Vis and FTIR spectra of the synthesized nanocomposites were also investigated to further support the synthesis of the nanocomposites. Cell parameter refinements of the synthesized nanocomposites were also investigated.

REFERENCES

1. Jawahara I.N., Mohanan P., Sebastian M.T., *Mat. Lett.*, **57** (2003), 4043.
2. Liou Y.C., Shiue W.H., Shih C.Y., *Mater. Sci. Eng. B*, **131** (2006), 142.
3. Weiden M., Grauel A., Norwig J., Horn S., Steglich F., *J. Alloys and Compounds.,* **218** (1995), 13.
4. Lee C.T., Oua C.C., Lin Y.C., Huanga C.Y., Su C.Y., *J. Europ. Ceram. Society*, **27** (2007), 2273.
5. Lichtenberg F., Herrnberger A., Wiedenmann K., *Progress in solid state chem.*, **36** (2008), 253.
6. Liou Y.C., Tsai W.C., Chen H.M., *Ceram. International*, **35** (2009), 2119.
7. Urabe H., Hisatomi T., Minegishi T., Kubota J., *Farad. Dis.*, **176** (2014), 213.
8. Ikeya T., Senna M., *J. Non-Cryst. Solids*, **105** (1988), 243.
9. Ristic M., Popovic S., Music S., *Mater. Lett.*, **58** (2004), 2658.
10. Brayner R., Verduraz F.B., *Phys. Chem. Chem. Phys.*, **5** (2003), 1457.
11. Jehng J.M., Wachs I.E., *Chem. Mater.*, **3** (1991), 100.
12. Jing Z., Wang C., Wang G., Li W., Lu D., *J. Sol-Gel Sci. Technol.*, **56** (2010), 121.
13. Kim Y.H., Lee D.K., Cha H.G., Kim C.W., Kang Y.S., *J. Phys. Chem. C*, **111** (2007), 3629.
14. Angel J., Greena M., Karuppasamy K., Antony R., Shajan X.S., Kumaresan S., *Chem. Sci. Trans.*, **2** (2013), 141.
15. Hsin-Yu Lin., Hsien-Chang Y., Wei-Lin W., *Catal. Today*, **174** (2011), 106.
16. Chen D., Ye J., *Chem. Mater.*, **21** (2009), 2327.